

# miR398b and *AtC2GnT* form a negative feedback loop to regulate *Arabidopsis thaliana* resistance against *Phytophthora parasitica*

Xiuhong Gou<sup>1</sup>, Chengcheng Zhong<sup>1</sup>, Peiling Zhang<sup>2</sup>, Liru Mi<sup>2</sup>, Yilin Li<sup>2</sup>, Wenqin Lu<sup>1</sup>, Jie Zheng<sup>2</sup>, Junjie Xu<sup>1</sup>, Yuling Meng<sup>2</sup> and Weixing Shan<sup>2,\*</sup> 

<sup>1</sup>State Key Laboratory of Crop Stress Biology for Arid Areas and College of Plant Protection, Northwest A&F University, Yangling, Shaanxi 712100, China, and

<sup>2</sup>State Key Laboratory of Crop Stress Biology for Arid Areas and College of Agronomy, Northwest A&F University, Yangling, Shaanxi 712100, China

Received 11 April 2022; revised 28 April 2022; accepted 2 May 2022

\*For correspondence (e-mail wxshan@nwfau.edu.cn).

## SUMMARY

Oomycetes are diploid eukaryotic microorganisms that seriously threaten sustainable crop production. MicroRNAs (miRNAs) and corresponding natural antisense transcripts (NATs) are important regulators of multiple biological processes. However, little is known about their roles in plant immunity against oomycete pathogens. In this study, we report the identification and functional characterization of miR398b and its *cis*-NAT, the *core-2/l-branching beta-1,6-N-acetylglucosaminyltransferase* gene (*AtC2GnT*), in plant immunity. Gain- and loss-of-function assays revealed that miR398b mediates *Arabidopsis thaliana* susceptibility to *Phytophthora parasitica* by targeting *Cu/Zn-Superoxidase Dismutase1* (*CSD1*) and *CSD2*, leading to suppressed expression of *CSD1* and *CSD2* and decreased plant disease resistance. We further showed that *AtC2GnT* transcripts could inhibit the miR398b–*CSDs* module via inhibition of pri-miR398b expression, leading to elevated plant resistance to *P. parasitica*. Furthermore, quantitative reverse transcription PCR, RNA ligase-mediated 5'-amplification of cDNA ends (RLM-5' RACE), and transient expression assays indicated that miR398b suppresses the expression of *AtC2GnT*. We generated *AtC2GnT*-silenced *A. thaliana* plants by CRISPR/Cas9 or RNA interference methods, and the *Nicotiana benthamiana* *Nbc2GnT*-silenced plants by virus-induced gene silencing. Pathogenicity assays showed that the *C2GnT*-silenced plants were more susceptible, while *AtC2GnT*-overexpressing plants exhibited elevated resistance to *P. parasitica*. *AtC2GnT* encodes a Golgi-localized protein, and transient expression of *AtC2GnT* enhanced *N. benthamiana* resistance to *Phytophthora* pathogens. Taken together, our results revealed a positive role of *AtC2GnT* and a negative regulatory loop formed by miR398b and *AtC2GnT* in regulating plant resistance to *P. parasitica*.

**Keywords:** *Arabidopsis thaliana*, oomycetes, *Phytophthora parasitica*, miR398, *AtC2GnT*, plant immunity, natural antisense transcripts.

## INTRODUCTION

Oomycete pathogens are a major factor causing serious damage to a wide range of plants, threatening sustainable crop production. *Phytophthora* is a well-known 'plant destroyer' in terms of its genetic variability and plasticity in overcoming host plant genotype-specific disease resistance. The management of many crop diseases caused by *Phytophthora* strongly relies on fungicide application (Judelson & Blanco, 2005; Kamoun et al., 2015; Thines & Kamoun, 2010). Therefore, understanding of plant susceptibility to oomycete pathogens is essential for developing novel strategies to improve plant disease resistance.

MicroRNAs (miRNAs), a class of small non-coding RNAs (sRNAs), play regulatory roles at post-transcriptional levels via guiding target mRNA degradation or translation inhibition in a sequence-specific manner (Jones-Rhoades et al., 2006; Yu et al., 2017). An increasing body of evidence suggests that endogenous plant sRNAs are involved in the interaction between host plant and pathogens (Katiyar-Agarwal & Jin, 2010; Šević et al., 2021; Song et al., 2021), including *Arabidopsis thaliana* miRNAs that were identified to be differentially responsive to *Phytophthora* pathogens by comparing high-throughput sRNA sequencing data (Zhong, 2019; Zhu et al., 2020).

*Arabidopsis thaliana* miR398b differentially accumulated upon *Phytophthora parasitica* (Zhong, 2019) and *Phytophthora capsici* (Zhu et al., 2020) infection. miR398 is a conserved miRNA family and has been reported to suppress expression of superoxidase dismutase (SOD) family members to regulate the plant immune response to multiple plant pathogens, including bacteria, fungi, and viruses (Li et al., 2010; Li, Cao, et al., 2019; Lin et al., 2022; Xu et al., 2014). For example, miR398 negatively regulates *A. thaliana* resistance to *Pseudomonas syringae* pv. *tomato* (*Pst*) DC3000 by suppressing expression of *Cu/Zn-SOD1* (*CSD1*) and *CSD2* (Jagadeeswaran et al., 2009; Li et al., 2010); *Osa*-miR398b positively regulates rice (*Oryza sativa*) resistance against *Magnaporthe oryzae* by repressing the expression of *CSD1*, *CSD2*, *Superoxide DismutaseX* (*SODX*), and *Copper Chaperone for Superoxide Dismutase* (*CCSD*) (Li et al., 2014; Li, Cao, et al., 2019); *Nb*-miR398 negatively regulates *Nicotiana benthamiana* immunity to Bamboo mosaic virus (BaMV), while *NbCSD2* functions as a positive regulator of *N. benthamiana* immunity against BaMV (Lin et al., 2022). However, whether miR398 participates in regulating plant immunity against oomycete pathogens remains largely elusive.

Natural antisense transcripts (NATs) are a class of endogenous regulatory RNA molecules that are partially or perfectly complementary to other transcripts (Wang et al., 2005). NATs can be divided into two groups, *trans*- and *cis*-NATs, based on the genomic locus. The former are transcribed from genomic loci that are distinct from their corresponding sense genes, while the latter are transcribed from the opposite strands of the same genomic locus (Mao et al., 2021; Wang et al., 2005). NATs participate in multiple gene regulation events, such as RNA editing, RNA masking, chromatin changes, and RNA interference (RNAi) (Jin et al., 2008; Rosikiewicz & Makalowska, 2016; Wight & Werner, 2013). A growing number of studies have revealed that miRNAs and their corresponding NATs are involved in a broad range of stress responses (Jiang et al., 2020; Li et al., 2020; Yu et al., 2013). For instance, Yu et al. (2013) identified eight heat-responsive *Brassica rapa* *cis*-NATs corresponding to precursors of *MIRNA* genes; Jiang et al. (2020) revealed that *Sl-lncRNA15492* and *Sl-miR482a* form a negative regulatory loop involved in the *Solanum lycopersicum* immune response to *Phytophthora infestans*. However, whether miRNAs and their corresponding NATs play regulatory roles in plant resistance against oomycete pathogens remains unresolved.

The locus *MIR398b* (*At5G14545*) is located on chromosome 5 in the *A. thaliana* genome, overlapping with the distal sequence of the 3'-untranslated region (3'-UTR) from the opposite strand-encoded gene *AtC2GnT* (*At5G14550*) (Li et al., 2020). *AtC2GnT* (also known as *NAT398b*), transcribed in the reverse direction of *MIR398b*, is the *cis*-NAT of *MIR398b* (Li et al., 2020). The overlapping region

between the *AtC2GnT* 3'-UTR and pri-miR398b can form an RNA duplex and generate *cis*-NAT-derived small interfering RNAs (nat-siRNAs) to impair the stability and accurate processing of pri-miR398b, leading to the upregulation of *CSD1* and *CSD2* and attenuated plant thermotolerance (Li et al., 2020). However, whether miR398b and *AtC2GnT* play regulatory roles in plant immunity to oomycete pathogens remains unresolved.

In this study, we showed that (i) miR398b mediates *A. thaliana* susceptibility against *P. parasitica* via suppressing expression of *CSD1*, *CSD2*, and *AtC2GnT* and (ii) *CSD1*, *CSD2*, and *AtC2GnT* positively regulate plant resistance. Moreover, we showed that *AtC2GnT* transcripts mediate *A. thaliana* resistance to *P. parasitica* via suppressing the miR398b–*CSDs* pathway, while the *AtC2GnT* protein-mediated plant resistance against *P. parasitica* is independent of the miR398b–*CSDs* route. Taken together, we reveal a positive role of *AtC2GnT* independent of miR398b and a negative regulatory loop formed by miR398b and *AtC2GnT* in regulating plant resistance to *P. parasitica*.

## RESULTS

### miR398b negatively regulates *A. thaliana* immunity to *P. parasitica*

*Arabidopsis thaliana* miR398b was identified to accumulate differentially upon *P. parasitica* infection by analyzing high-throughput sRNA sequencing data of *P. parasitica*-infected *A. thaliana* roots (Zhong, 2019). We confirmed the accumulation of miR398b in both root and leaf tissues upon *P. parasitica* infection via stem-loop quantitative reverse transcription PCR (qRT-PCR) analysis. Consistently, the miR398b levels in root and leaf tissues were both reduced during *P. parasitica* infection (Figure 1a,b). We thus hypothesized that miR398b may participate in regulating *A. thaliana* immunity.

To investigate the immune function of miR398b to *P. parasitica*, we generated transgenic miR398b-silenced and miR398b overexpression plants in *A. thaliana* ecotype Columbia-0 (Col-0). The miR398b-silenced transgenic plants were generated by using the G:U hpRNA sponge as described by Zhong (2019). Two independent transgenic lines (*mir398-1* and *mir398-5*), in which the expression of miR398b was reduced by more than 90%, were identified and selected for further analysis (Figure 1c). In the transgenic *Arabidopsis* plants overexpressing pre-miR398b, the miR398b precursor under the transcriptional control of the cauliflower mosaic virus (CaMV) 35S promoter (Li et al., 2010), the RNA levels of miR398b and pre-miR398b were measured by stem-loop qRT-PCR and qRT-PCR, respectively (Figure 1d). Two individual transgenic lines with confirmed miR398b overexpression, *MIR398b-OE3* and *MIR398b-OE6*, were selected for further analysis. The results indicated that the expression of *CSD1* and *CSD2*,

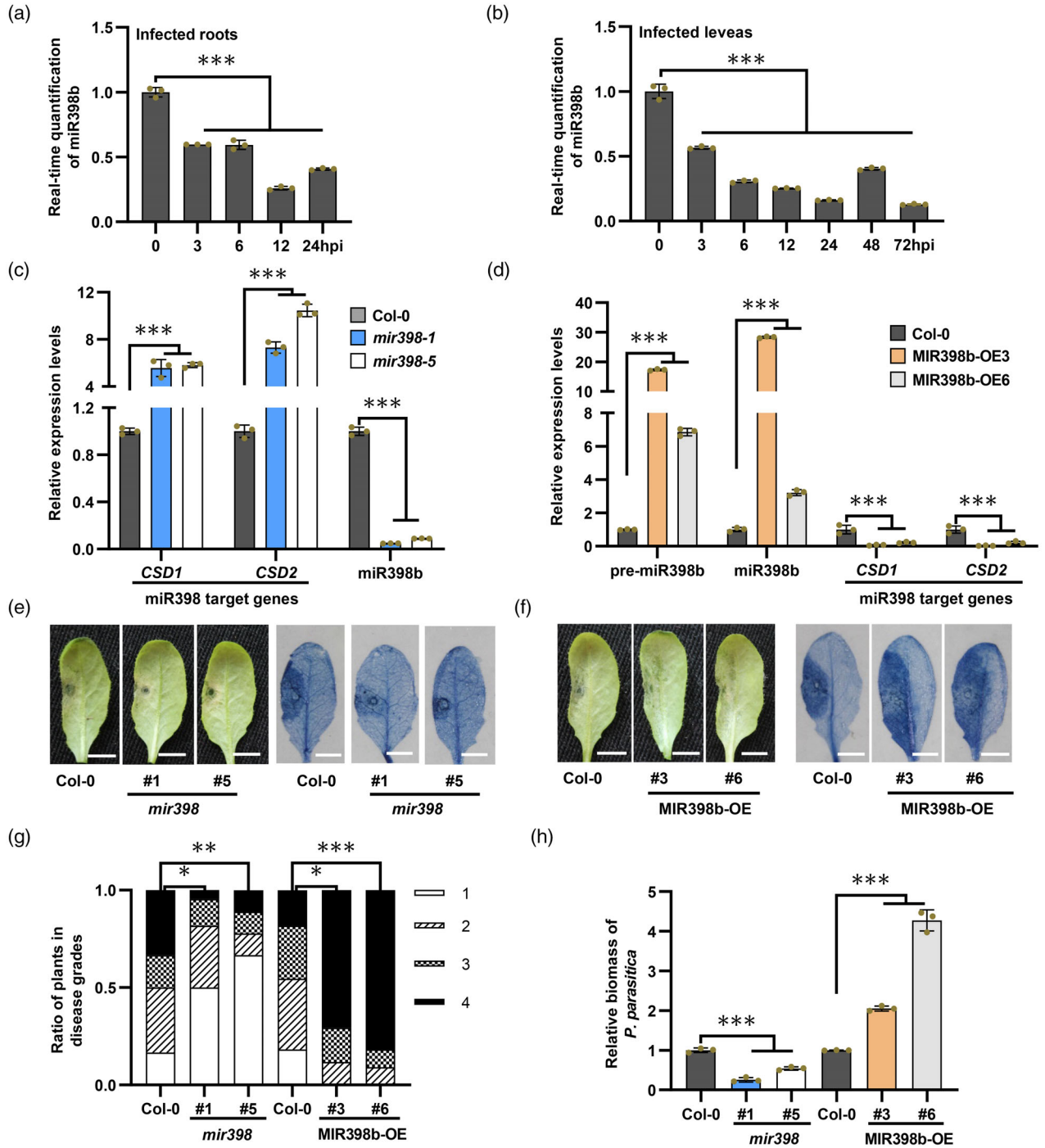


**Figure 1.** miR398b negatively regulates plant immunity to *Phytophthora parasitica*.

(a, b) Real-time quantification of miR398b in *P. parasitica*-infected *Arabidopsis thaliana* roots (a) and leaves (b) by stem-loop quantitative reverse transcription PCR (qRT-PCR), with *A. thaliana U6 (AtU6)* serving as an internal reference.

(c, d) Relative expression levels of the related genes in miR398b-silenced transgenic plants (c) and miR398b overexpression transgenic plants (d).

(e, f) Four-week-old detached leaves of miR398b-silenced and miR398b overexpression transgenic plants and wild-type Col-0 were inoculated with *P. parasitica* zoospores. The photographs of infected leaves were taken at 3 days post-inoculation (dpi). The infected leaves were stained with trypan blue to highlight the lesions. Scale bars: 5 mm.

(g) Plant disease severity was scored based on the colonization area ratio of *P. parasitica* at 3 days post-inoculation (dpi). Grade 1, 0–10%; Grade 2, 10–33%; Grade 3, 33–66%; Grade 4, 66–100%. The statistical analysis was based on the Wilcoxon rank-sum test. At least three independent experiments gave similar results.

(h) Biomass of *P. parasitica* in infected leaves was measured by quantitative PCR (qPCR). Data are presented as the mean  $\pm$  SD ( $n = 3$ ). The statistical analysis of (a–d) and (h) was based on Student's *t*-test. Asterisks indicate significant differences (\* $P < 0.05$ , \*\* $P < 0.01$ , \*\*\* $P < 0.001$ ).

two target genes of miR398 (Brodersen et al., 2008; Sunkar et al., 2006), was upregulated when miR398b was downregulated and downregulated when miR398b was overexpressed (Figure 1c,d). When 4-week-old detached rosette leaves were inoculated with *P. parasitica* zoospores, the scoring results at 3 days post-inoculation (dpi) clearly showed that compared to the wild type (Col-0), *mir398-1* and *mir398-5* developed smaller lesions, while MIR398b-OE3 and MIR398b-OE6 showed larger lesions (Figure 1e–g). Consistently, relative to wild-type Col-0, significantly less pathogen colonization was detected in *mir398-1* and *mir398-5* plants, but the opposite was true for MIR398b-OE3 and MIR398b-OE6 lines (Figure 1h). These corroborating results manifest that miR398b negatively regulates *A. thaliana* immunity against *P. parasitica*.

Considering the miR398–CSDs module plays multiple roles in diverse plant–pathogen interactions (Li, Cao, et al., 2019; Lin et al., 2022; Xu et al., 2014), we explored its potential involvement in plant immune response to *P. parasitica* by performing pathogenicity assays on the detached leaves of *csd1* and *csd2*, which are the insertional mutants of *CSD1* and *CSD2*, respectively. It is clearly shown that both *csd1* and *csd2* were more susceptible than wild-type Col-0 (Figure S1), indicating that silencing of *CSD1* and *CSD2* enhanced plant susceptibility to *P. parasitica*.

#### miR398b suppresses *AtC2GnT* expression

The miR398b sequence is reverse complementary to the 3'-UTR of the antisense gene *AtC2GnT* (Figure 2a), and thus could potentially induce the silencing of *AtC2GnT*. To elucidate whether *AtC2GnT* is the authentic target gene of miR398b, we examined the *AtC2GnT* transcript abundance in the aforementioned transgenic *A. thaliana* plants and in wild type (Col-0) by qRT-PCR. Compared to the wild type, the *AtC2GnT* expression levels were upregulated in *mir398-1* and *mir398-5* plants and downregulated in MIR398b-OE3 and MIR398b-OE6 plants (Figure 2b). Furthermore, the difference was more significant at 72 h post-inoculation (hpi) with *P. parasitica* (Figure 2c). To verify whether the alteration of *AtC2GnT* transcript levels was due to the mRNA cleavage guided by miR398b, we performed an RNA ligase-mediated 5'-amplification of cDNA ends (RLM-5' RACE) assay. The canonical cleavage site of the target gene is usually located between the nucleotides that pair with the 10th and 11th nucleotides of the miRNAs (Jones-Rhoades et al., 2006). The results showed that the miR398b-guided *AtC2GnT* mRNA cleavage site was located at the 36th base upstream of the predicted canonical cleavage site (Figure 2d; Figure S2). Previous studies have also reported this type of non-canonical cleavage phenomena, such as the miR844-guided *Cytidinephosphate Diacylglycerol Synthase3* (*CDS3*) mRNA cleavage (Lee et al., 2015) and the miR840- and miR840\*-guided cleavage of

*WHIRLY3* (*WHY3*) and *PPR* mRNA, respectively (Ren et al., 2022).

Furthermore, we designed a GFP-based reporter assay to verify the cleavage site. Given that the target site of miR398b was located in the 3'-UTR of *AtC2GnT*, we designed CaMV 35S-driven constructs in which GFP was fused to a truncated *AtC2GnT* that includes the 3'-UTR (GFP-wtUTR) or a mutated truncated *AtC2GnT* with an altered miR398b target site (GFP-muUTR) (Figure 2e). The constructs were transiently co-expressed with *p35S::mir398b* in *N. benthamiana* leaves via *Agrobacterium tumefaciens*-mediated transformation. GFP expression was determined by both fluorescence intensity and Western blot analyses. Both quantitation methods indicated that when expressed alone, GFP-wtUTR and GFP-muUTR proteins were highly abundant. However, when co-expressed with *p35S::mir398b*, the protein level of GFP-wtUTR but not that of GFP-muUTR was significantly reduced, especially at high concentrations of the infiltrated *Agrobacterium* (Figure 2f,h). It is therefore evident that miR398b suppresses *AtC2GnT* expression via targeting the *AtC2GnT* 3'-UTR.

Since *AtC2GnT* overlaps with *MIR398b* in the pri-miR398b region (Figure 2a), pri-miR398b and the 3'-UTR of *AtC2GnT* can potentially form double-stranded RNA (dsRNA) and generate nat-siRNAs, which might further degrade pri-miR398b through siRNA-induced gene silencing (Li et al., 2020), which might explain the downregulation of GFP-wtUTR when *p35S::mir398b* and *p35S::GFP-wtUTR* were co-expressed. To further clarify the difference between pri-miR398b and miR398b in suppressing *AtC2GnT* expression, we generated an artificial miR398b (amiR398b) vector with a *MIR319a* backbone (Schwab et al., 2006). When co-expressed with amiR398b, the protein level and the fluorescence intensity of GFP-wtUTR, but not those of GFP-muUTR, were reduced significantly (Figure 2g,i), indicating that mature miR398b can suppress *AtC2GnT* expression. Taken together, these results enabled the identification of the *AtC2GnT* 3'-UTR as the target site for miR398b suppression and confirmed the miR398b-guided non-canonical cleavage of *AtC2GnT*.

#### Mutation and manipulation of *AtC2GnT* expression significantly alter plant immunity to *P. parasitica* infection

To further explore the function of *AtC2GnT* in the interaction between *A. thaliana* and *P. parasitica*, we generated independent *AtC2GnT* knockout mutants by using CRISPR/Cas9-based technology (Mao et al., 2013). A homozygous mutant, named *c2gnt*, was obtained at the T2 generation. *c2gnt*, with a 1-bp insertion in the single-stranded guide RNA1 (sgRNA1) target site, encodes a truncated *AtC2GnT* protein (Figure 3a). The qRT-PCR results revealed that the insertion in the *c2gnt* mutant had no effect on the mRNA expression of *AtC2GnT* (Figure 3b). For comparison, we

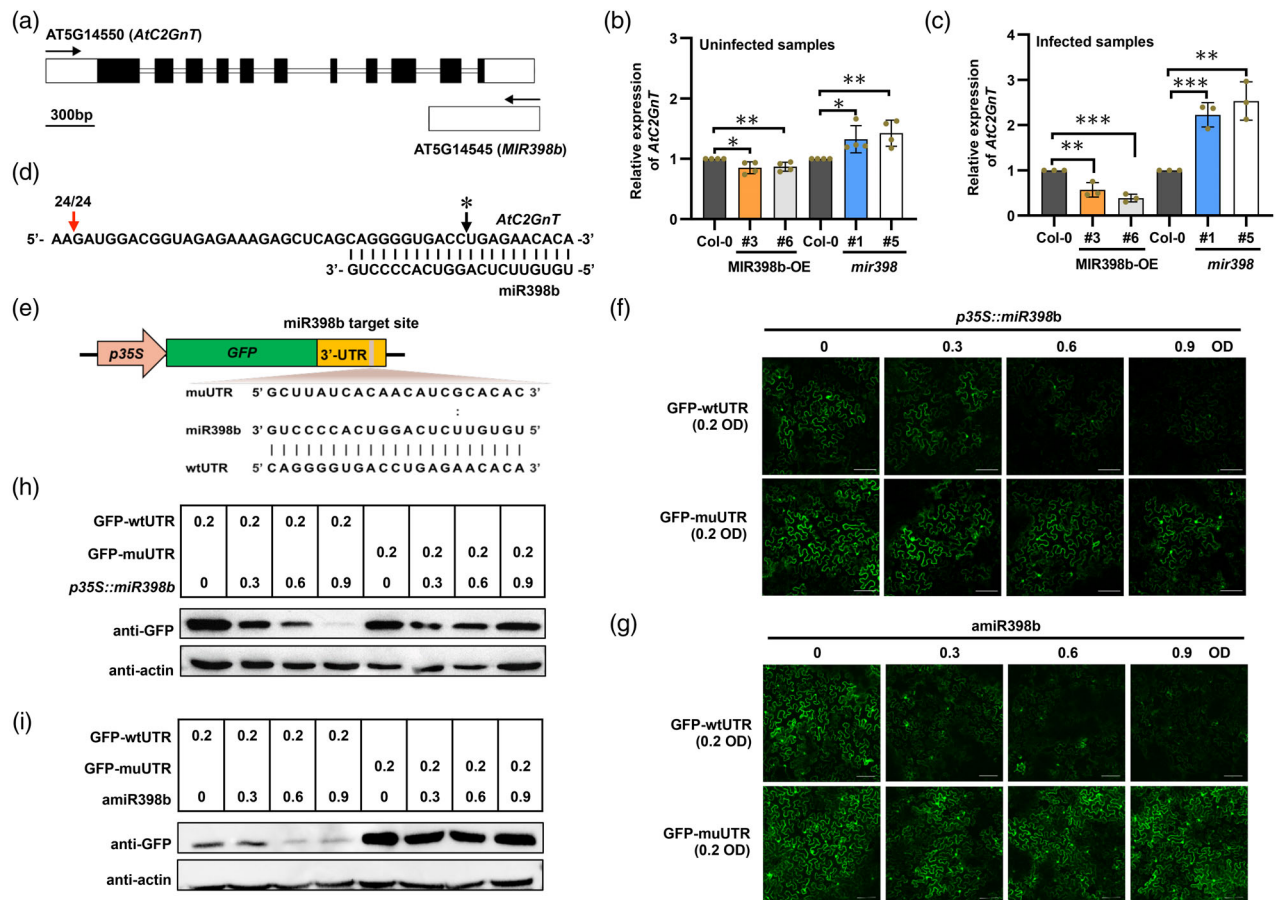


**Figure 2.** miR398b suppresses the expression of *AtC2GnT*.

(a) Schematic structures and genomic location of *AtC2GnT* and *MIR398b* in *Arabidopsis thaliana*. The black arrows indicate transcript directions; the black boxes indicate the exons.

(b) Relative expression levels of *AtC2GnT* in the indicated lines uninfected with *Phytophthora parasitica*. Data are presented as the mean  $\pm$  SD ( $n = 4$ ).

(c) The expression levels of *AtC2GnT* in the indicated lines at 72 h post-inoculation (hpi) with *P. parasitica*. Data are presented as the mean  $\pm$  SD ( $n = 3$ ). The asterisks in (b, c) indicate significant differences based on Student's *t*-test (\* $P < 0.05$ , \*\* $P < 0.01$ , \*\*\* $P < 0.001$ ).

(d) RLM-5' RACE assay of *AtC2GnT*. The red arrow shows the cleavage site. Out of 24 cloned sequences, all 24 contained the same cleavage site; the black arrow with an asterisk shows the predicted miR398b canonical cleavage site.

(e) Nucleotide sequences of the wild-type 3'-UTR (wtUTR) and mutated 3'-UTR (muUTR) versions of *AtC2GnT* aligned against the miR398b sequence.

(f, g) The constructs containing *p35S::GFP-wtUTR* or *p35S::GFP-muUTR* were separately expressed or co-expressed with *p35S::miR398b* (f) or *amiR398b* (g) in *Nicotiana benthamiana* leaves using *Agrobacterium*-mediated infiltration at the indicated OD<sub>600</sub> value. Confocal images revealing the fluorescence intensities of GFP-wtUTR and GFP-muUTR were taken with an Olympus FV3000 confocal microscopy. Size bars: 100  $\mu$ m.

(h, i) The protein levels of GFP were detected by Western blot analysis; actin was used as the loading control. The experiments were repeated at least two times with similar results.

also generated two *AtC2GnT* knockdown transformants by RNAi, named RNAi-8 and RNAi-20 (Figure S3a). Pathogenicity assays on 4-week-old detached leaves with *P. parasitica* zoospores showed that significantly larger lesions were formed in *c2gnt* mutant and RNAi transgenic lines than in the wild type (Col-0) (Figure 3d,f; Figure S3b, c). These results were corroborated by *P. parasitica* biomass quantification, which revealed much more pathogen colonization in the *c2gnt* mutant and RNAi transgenic lines compared to the wild type (Col-0) (Figure 3g; Figure S3d). Taken together, these results indicated that the attenuation of *AtC2GnT* could compromise *A. thaliana* resistance against *P. parasitica*.

It has been commonly recognized that the expression of a sense transcript can be stimulated or attenuated by NATs (Wight & Werner, 2013). In RNAi transgenic *A. thaliana*, the expression of pri-miR398b and miR398b was enhanced, resulting in downregulation of *CSD1* and *CSD2* (Figure S4a), while no significant variation was detected in the *c2gnt* mutant (Figure S4b). This is in congruence with a previous study which revealed that *AtC2GnT* transcripts, rather than *AtC2GnT* proteins, reduced plant thermotolerance by impairing expression of pri-miR398b and enhancing expression of *CSD1* (Li et al., 2020). It is therefore conceivable that *AtC2GnT* transcripts play an imperative role in *A. thaliana* resistance to *P. parasitica* by regulating

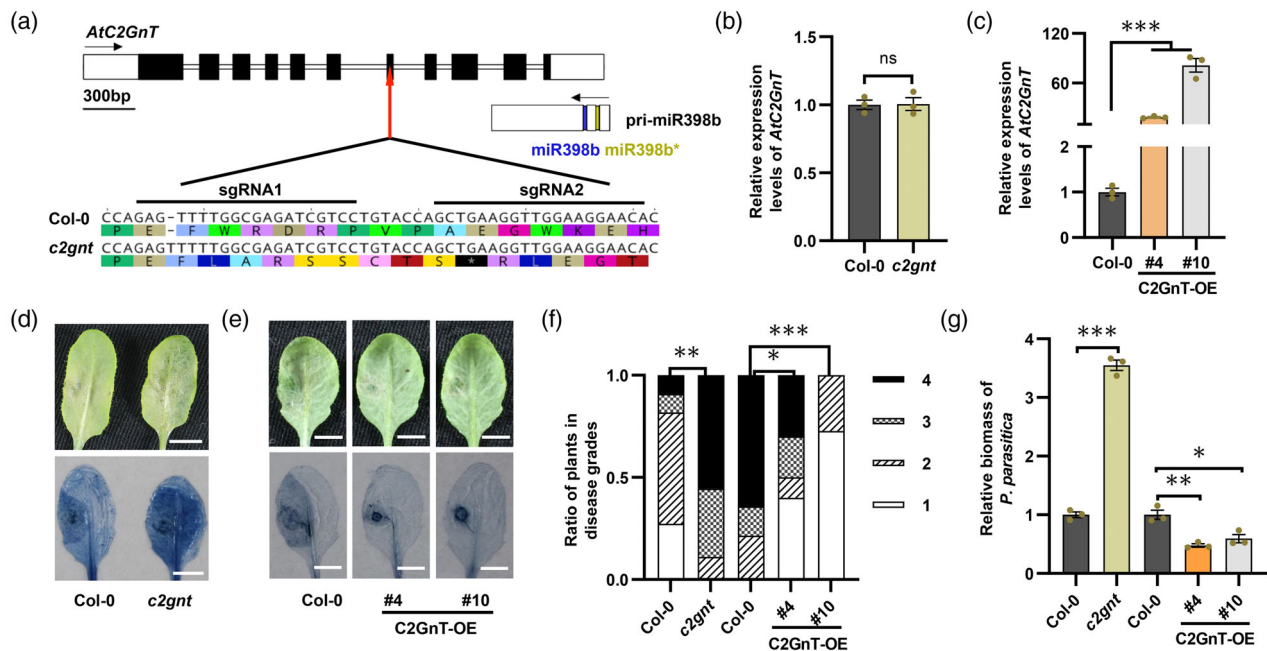


**Figure 3.** *AtC2GnT* is a positive regulator of *Arabidopsis thaliana* immunity to *Phytophthora parasitica*. (a) Schematic edit positions and representative sequence of CRISPR/Cas9-edited mutant. The black arrows indicate transcript directions; the black boxes indicate exons; the red arrow indicates the edit position. (b, c) The expression levels of *AtC2GnT* in *c2gnt* mutant (b) and *AtC2GnT* overexpression transgenic plants (c) were measured by quantitative reverse transcription PCR (qRT-PCR). *AtUBC9* was used as a reference gene. (d, e) The disease symptoms of the *c2gnt* mutant (d) and *AtC2GnT* overexpression transgenic plants (e) inoculated with *P. parasitica* zoospores were photographed at 3 days post-inoculation (dpi). The infected leaves were stained with trypan blue to highlight the lesions. Scale bars: 5 mm. (f) Statistical analysis of plant disease grades. The evaluation and statistical analysis of plant disease grades were performed as described in Figure 1(g). The *P. parasitica* biomass in infected leaves at 3 days post-inoculation (dpi) was determined by qPCR. Data are presented as the mean  $\pm$  SD ( $n = 3$ ). The statistical analysis of (b, c) and (g) was based on Student's *t*-test. Asterisks above the bars indicate significant differences (\* $P < 0.05$ , \*\* $P < 0.01$ , \*\*\* $P < 0.001$ ; ns, no significance).

the miR398b–CSDs module, while the enhanced susceptibility of the *c2gnt* mutant to *P. parasitica* is independent of the miR398b–CSDs module.

To further reveal the function of *AtC2GnT* in plant resistance, we generated an *AtC2GnT* overexpression construct carrying the *AtC2GnT* coding sequence (CDS) without its native 3'-UTR sequence which contains the miR398b target site. We transformed *A. thaliana* ecotype Col-0 with this *AtC2GnT* overexpression construct via the floral dip method (Zhang et al., 2006). Two independent transgenic lines, C2GnT-OE4 and C2GnT-OE10, were selected for further analysis. qRT-PCR analysis (Figure 3c) revealed that the expression of *AtC2GnT* in C2GnT-OE4 and C2GnT-OE10 was significantly enhanced. In our pathogenicity assays on 4-week-old detached leaves with *P. parasitica* zoospores, smaller lesions were observed in C2GnT-OE4 and C2GnT-OE10 plants relative to the wild type (Col-0) (Figure 3e,f). Consistent results were obtained in the biomass quantification experiments, where the *AtC2GnT* overexpression lines had less *P. parasitica* biomass compared to the wild type (Col-0) (Figure 3g). These results indicated that overexpression of *AtC2GnT* inhibited lesion expansion

and *P. parasitica* colonization. The expression of miR398b and CSDs in both C2GnT-OE4 and C2GnT-OE10 plants showed no significant variation compared to the wild type (Col-0) (Figure S4c), indicating that overexpression of the *AtC2GnT* CDS does not influence the expression of miR398b–CSDs. This is in accordance with a previous study which reported that the *AtC2GnT* 3'-UTR, which is reverse complementary with the pri-miR398b sequence, is crucial for the expression of pri-miR398b (Li et al., 2020). These results confirmed that the enhanced resistance of transgenic *AtC2GnT* overexpression plants against *P. parasitica* is independent of the miR398b–CSDs pathway.

In conclusion, *AtC2GnT* leverages two independent routes to positively regulate plant disease resistance, with one route being dependent on the miR398b–CSDs module and the other being independent of the miR398b–CSDs module. Furthermore, transient expression of the *AtC2GnT* CDS in *N. benthamiana* leaves rendered plants more resistant to both *P. parasitica* and *P. infestans*, as shown by the smaller lesions, suggesting that *AtC2GnT* is functional in heterologous plant species against *Phytophthora* pathogens (Figure S5).

### AtC2GnT encodes a Golgi-localized protein

Although several NATs have been reported to encode proteins, the majority of NATs in eukaryotes are commonly considered non-coding (Jabnourne et al., 2013; Jiang et al., 2021; Mao et al., 2021; Su et al., 2012). The question naturally arises as to whether *AtC2GnT*, the *cis*-NAT of *MIR398b*, is protein-coding. To answer this question, we designed the *p35S::C2GnT-GFP* construct, which was transiently expressed in *N. benthamiana* leaves. Punctate green fluorescence signals were apparent in the *Agrobacterium*-infiltrated leaf areas as revealed by confocal microscopy analysis (Figure S6). Furthermore, transient expression of C2GnT-GFP in *N. benthamiana* leaves rendered plant cells more resistant to *P. parasitica* infection (Figure 4e,f), as indicated by the relatively small lesion areas, which also suggest that GFP fusion has no influence on AtC2GnT function. In addition, the C2GnT-GFP protein with the anticipated fusion size was detected by Western blot (Figure 4a).

*AtC2GnT* was predicted to encode a core-2/*l*-branching beta-1,6-*N*-acetylglucosaminyltransferase, which belongs to the GT14/GT14-like family of the glycosyltransferase (GT) superfamily (Figure S7). GTs are usually localized in the Golgi apparatus (Ye et al., 2011). To analyze the cellular localization of AtC2GnT, the C2GnT-GFP fusion construct was co-transformed into *N. benthamiana* leaves with the RFP-labeled Golgi apparatus marker CTS-RFP (Strasser et al., 2006). The overlap of the green fluorescence signal of C2GnT-GFP and the red fluorescence signal of CTS-RFP illustrated the localization of C2GnT-GFP to the Golgi apparatus (Figure 4b).

Structural prediction by TMHMM2.0 suggested that AtC2GnT contains a transmembrane helix (T) that links a short cytoplasmic N-terminus (N) and a long non-cytoplasmic C-terminus (C) (Figure S8). The resident proteins of the Golgi apparatus contain localization signals to ensure correct subcellular targeting and transportation without being swept along the biosynthetic pathway (Teasdale et al., 1994). To determine the regions or domains that are crucial for Golgi targeting and retention, we constructed a series of AtC2GnT deletion mutants with GFP fused to their C-termini (Figure 4c). The deletion mutants were co-transformed into *N. benthamiana* leaves with CTS-RFP and the subcellular localizations of these deletion mutants were examined by confocal microscopy. The punctate fluorescence signals of TC-GFP and C-GFP overlapped with the CTS-RFP signal (Figure 4d). The fluorescence signal of NT-GFP partially overlapped with CTS-RFP and the endoplasmic reticulum (ER) marker ER-mCherry (Fan et al., 2018) (Figure 4d; Figure S9). In contrast, the fluorescence signal of N-GFP did not discernably overlap with CTS-RFP (Figure 4d), suggesting the absence of the Golgi targeting domain in region N, while region T and region C

may harbor the crucial domains for Golgi targeting and retention.

To assign the immune function of AtC2GnT to the N, T, and C regions, we examined the functional roles of their GFP fusions, TC-GFP, C-GFP, NT-GFP, and N-GFP, in plant immunity against *P. parasitica* via transient overexpression and pathogenicity assays in *N. benthamiana*. As is evident in Figure 4(e,f), all AtC2GnT deletion mutants except TC-GFP lost their ability to enhance resistance to *P. parasitica* colonization, suggesting that regions T and C, but not region N, of AtC2GnT are indispensable for the immune role against *P. parasitica*.

### Silencing of *NbC2GnT* by virus-induced gene silencing reduced *N. benthamiana* resistance to *Phytophthora* pathogens

C2GnT is a conserved protein in plants. To examine whether the immune function of *C2GnT* is conserved across different plant species, we investigated its homologous genes in *N. benthamiana*. Two sequences, designated as *NbC2GnTA* (Niben101Scf11415g00001.1) and *NbC2GnTB* (Niben101Scf01448g02029.1), were identified in the *N. benthamiana* genome, encoding proteins with 60.7% and 59.68% sequence identities to AtC2GnT, respectively (Figure S10). Given the high sequence similarity between *NbC2GnTA* and *NbC2GnTB*, we co-silenced them by virus-induced gene silencing (VIGS) with a tobacco rattle virus (TRV) vector (Liu et al., 2002; Ratcliff et al., 2001). As a result, the expression of *NbC2GnTA* and *NbC2GnTB* was reduced by more than 90% in the VIGS plants transformed with *TRV2::NbC2GnT* (*tNbC2GnT*) compared to *TRV2::GFP* (*tGFP*) plants, as revealed by qRT-PCR analysis (Figure 5a). Pathogenicity assays on the detached leaves 3 weeks post-infiltration showed significantly larger lesions on the *tNbC2GnT* plants compared to the *tGFP* plants for both *P. parasitica* (Figure 5b,d) and *P. infestans* (Figure 5c,e), confirming that *NbC2GnT* may play a positive role in plant immunity. These results imply that C2GnT is a conserved positive immune regulator across distant plant species against *Phytophthora* pathogens, which warrants verification and further investigation in a wide range of plant species.

## DISCUSSION

Oomycetes, particularly *Phytophthora* spp., infect a variety of crops and forest seedlings worldwide, causing a plethora of severe agriculturally relevant diseases (Kamoun et al., 2015; Thines & Kamoun, 2010), which invokes research on the mechanisms of plant immunity. Plant miRNAs and *cis*-NATs have been reported to be involved in the plant innate immune system. The identification and utilization of the miRNAs and *cis*-NATs that participate in plant susceptibility regulation may provide a novel avenue to

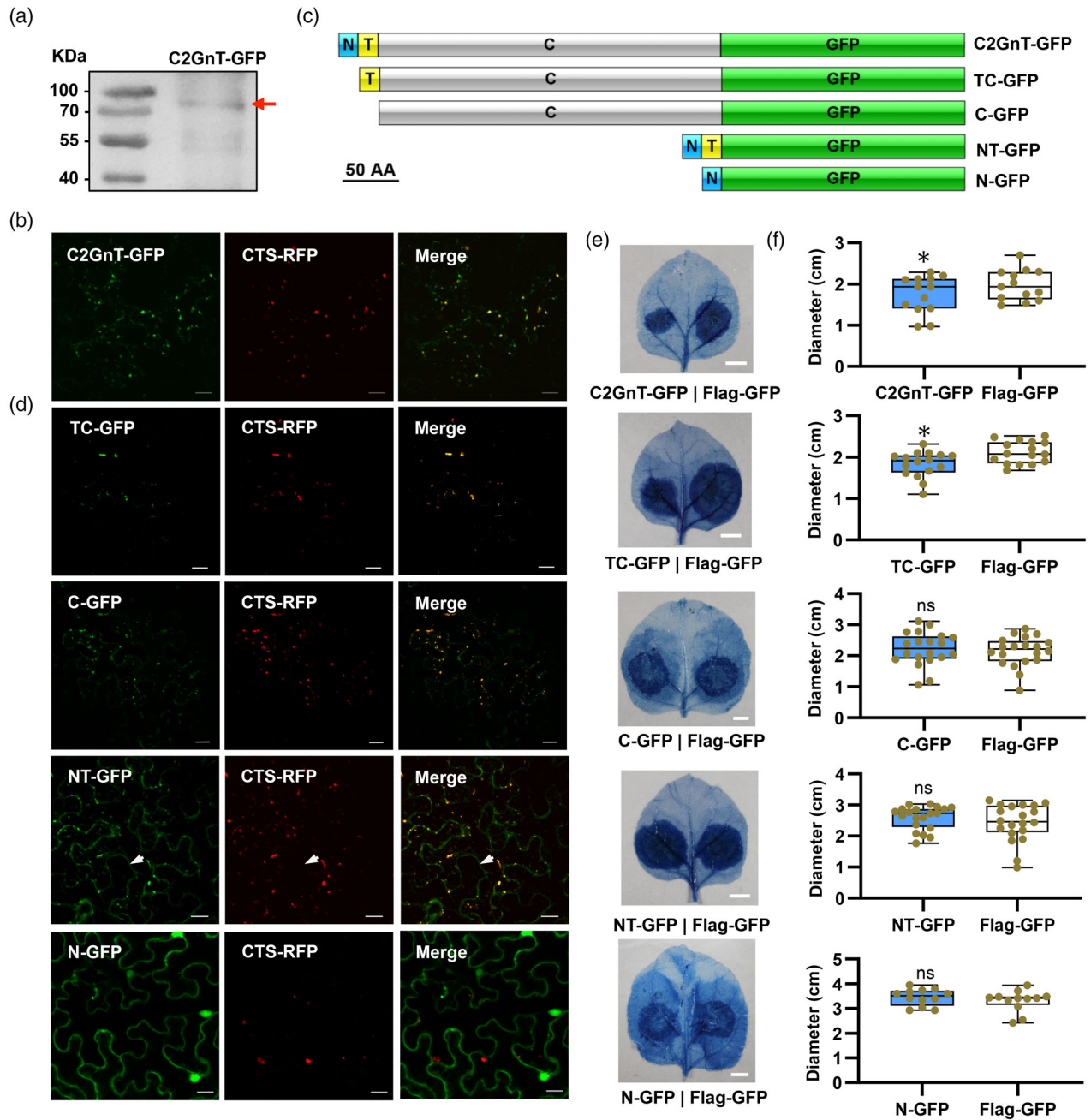


**Figure 4.** *AtC2GnT* encodes a Golgi-localized protein. (a) The protein expression of C2GnT-GFP was detected by Western blot. The red arrow represents the correct protein band of C2GnT-GFP (c. 71.54 kDa). (b) The C2GnT-GFP protein was localized in the Golgi. C2GnT-GFP co-localized with the Golgi marker CTS-RFP. Scale bar: 20  $\mu$ m. (c) Schematic diagrams of the *AtC2GnT* deletion mutants. N, N-terminal cytoplasmic domain; T, transmembrane helix; C, C-terminal non-cytoplasmic domain. (d) Subcellular localization of the *AtC2GnT* deletion mutants. Scale bar: 20  $\mu$ m. (e, f) *Nicotiana benthamiana* leaves infiltrated with *Agrobacterium tumefaciens* carrying *AtC2GnT* deletion mutants and Flag-GFP were inoculated with *Phytophthora parasitica*. The diameters of lesions were measured at 60 h post-inoculation (hpi) followed by trypan blue staining to highlight the lesions. Scale bar: 1 cm. More than 10 leaves were used for statistical analysis, based on Student's *t*-test. The bars outside the box indicate the maximum and minimum values, while the lines in the box show the upper quartile, median, and lower quartile. Asterisks above the bars indicate significant differences ( $*P < 0.05$ ; ns, no significance). At least three independent experiments yielded similar results.

understand the pathogenic mechanisms underpinning such usually devastating diseases and develop plant germplasm resources with broad-spectrum and durable resistance.

miR398, which participates in the plant stress regulatory network, is conserved in both monocots and dicots (Guan et al., 2013; Li, Cao, et al., 2019). Here, we employed the *A.*

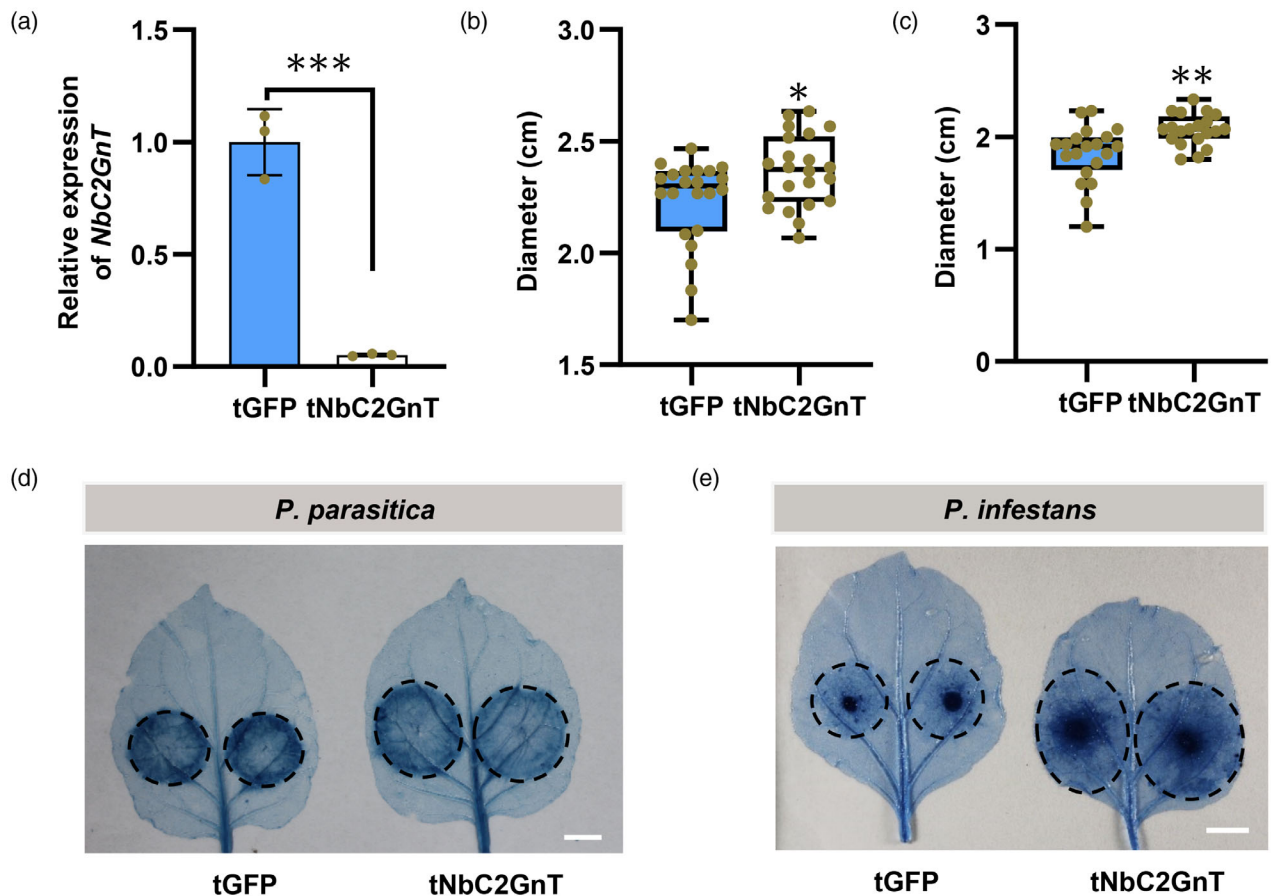


**Figure 5.** Silencing of *NbC2GnT* in *Nicotiana benthamiana* enhanced plant colonization by *Phytophthora parasitica* and *Phytophthora infestans*. (a) The gene expression levels of *NbC2GnTA* and *NbC2GnTB* in *TRV2::NbC2GnT* (*tNbC2GnT*) plants and *TRV2::GFP* (*tGFP*) plants were detected by quantitative reverse transcription PCR (qRT-PCR). *NbActin* served as the reference gene. The significance was assessed based on Student's *t*-test. (b, c) Boxplots showing the statistical analyses of lesion diameters in *tNbC2GnT* and *tGFP* leaves challenged with *P. parasitica* (b) and *P. infestans* (c). More than 10 leaves were used for statistical analysis based on Student's *t*-test. The bars outside the box indicate the maximum and minimum values, while the lines in the box show the upper quartile, median, and lower quartile. More than three independent experiments yielded similar results. (d, e) Trypan blue staining showing the lesions caused by *P. parasitica* (d) and *P. infestans* (e) that developed in *N. benthamiana* leaves. Scale bar: 1 cm. Asterisks indicate significant differences (\* $P < 0.05$ , \*\* $P < 0.01$ , \*\*\* $P < 0.001$ ).

*thaliana*–*P. parasitica* pathosystem to investigate the functionality of miR398b upon infection of *P. parasitica*. Transgenic plants with attenuated miR398b expression exhibited substantially ameliorated resistance to *P. parasitica*, whereas those overexpressing miR398b showed increased susceptibility (Figure 1), indicating that miR398b acts as a negative regulator of *A. thaliana* immunity against *P. parasitica*. Previous studies revealed that miR398b functions as a positive regulator in the rice immune response to *M. oryzae* (Li, Cao, et al., 2019), while miR398 plays a negative regulatory role in barley (*Hordeum vulgare*) resistance to powdery mildew (Xu et al., 2014), indicating that miR398 has multiple functions in diverse plant–pathogen interactions.

The regulatory effects of miR398 on target genes vary in diverse plant species (Li, Cao, et al., 2019; Lin et al., 2022; Liu et al., 2020; Xu et al., 2014). In this study, we revealed that miR398b suppresses *AtC2GnT* expression. Firstly,

qRT-PCR assays revealed a negative correlation between their expression levels (Figure 2b,c). Secondly, the results of our RLM-5' RACE assays indicated that miR398b guided non-canonical cleavage of *AtC2GnT* transcripts (Figure 2d; Figure S2). Thirdly, the transient expression assays indicated that mature miR398b guided *AtC2GnT* mRNA cleavage via identification of the target site located in the *AtC2GnT* 3'-UTR (Figure 2e-i). Our findings are incongruent with a previous study which reported that overexpression of miR398b had no influence on *AtC2GnT* expression (Li et al., 2020). A possible reason explaining such discrepancy is that the relationship between *AtC2GnT* and miR398b was influenced by the infection of *P. parasitica*. The *AtC2GnT* expression levels were less inhibited by miR398b in the uninfected plant tissues (Figure 2b), while the inhibition was more significant in the infected tissues (Figure 2c). A similar event has been reported in a previous

study. During the early stage of *Pst* (*avrRpt2*) infection, miR863-3p silences *atypical receptor-like pseudokinase1* (*ARLPK1*) and *ARLPK2*, while during the later stage of infection, miR863-3p silences *SERRATE* (Niu et al., 2016).

The functional role of *AtC2GnT* in the plant immune response to *P. parasitica* has so far not been elucidated. Here, we demonstrated that *AtC2GnT* serves as a positive regulator against *Phytophthora* infection in both *A. thaliana* and *N. benthamiana* (Figures 3 and 4; Figures S3 and S5). *cis*-NATs are usually associated with the downregulation of their corresponding sense genes (Jabnune et al., 2013). For example, the *cis*-NAT<sub>ZmNAC48</sub> negatively regulates the expression of *ZmNAC48*, leading to compromised drought tolerance in maize (*Zea mays*) (Mao et al., 2021); the *AtC2GnT* transcripts attenuated plant thermotolerance by impairing the expression of pri-miR398b and promoting the expression of *CSD1* (Li et al., 2020). Consistent with the previous studies, the expression of pri-miR398b and miR398b was enhanced in the RNAi transgenic *A. thaliana* plants, resulting in the downregulation of *CSDs*, while no significant variation was detected in the *c2gnt* mutant (Figure S4a,b). These results revealed that *AtC2GnT* transcripts, rather than the *AtC2GnT* protein, modulated *A. thaliana* resistance to *P. parasitica* dependent on the miR398b–*CSDs* module.

Furthermore, we found that *AtC2GnT* also regulates *A. thaliana* resistance against *Phytophthora* pathogens independently of miR398b. On the one hand, the *c2gnt* mutant and *AtC2GnT* overexpression transgenic plants showed no significant variation in expression of miR398b and *CSDs* compared to the wild-type Col-0 (Figure S4b,c), indicating the high susceptibility of the *c2gnt* mutant and the enhanced resistance of *AtC2GnT* overexpression transgenic plants against *P. parasitica* were independent of the miR398b–*CSDs* pathway. On the other hand, *AtC2GnT* encodes a Golgi-localized protein (Figure 4), and transient expression of the *AtC2GnT* CDS in *N. benthamiana* suppressed colonization of *Phytophthora* pathogens (Figure 4; Figure S5), indicating that *AtC2GnT* enhanced plant resistance in a way independent of the miR398b–*CSDs* module. Taken together, these results indicated that *AtC2GnT* leverages two independent routes to positively regulate disease resistance, with one route being dependent on the miR398b–*CSDs* module and the other being dependent on *AtC2GnT*, which also enhances plant resistance independently of the miR398b–*CSDs* module. Additionally, *C2GnT* and miR398 are conserved in *N. benthamiana*, and we demonstrated that silencing of *NbC2GnT* enhanced *N. benthamiana* susceptibility to *Phytophthora* pathogens (Figure 5). It is interesting to examine whether *N. benthamiana* miR398 (*Nb-miR398*) influences the function of *NbC2GnT* during the infection of *Phytophthora* pathogens. Future studies are warranted to clarify the relationship between *Nb-miR398* and *NbC2GnT*.

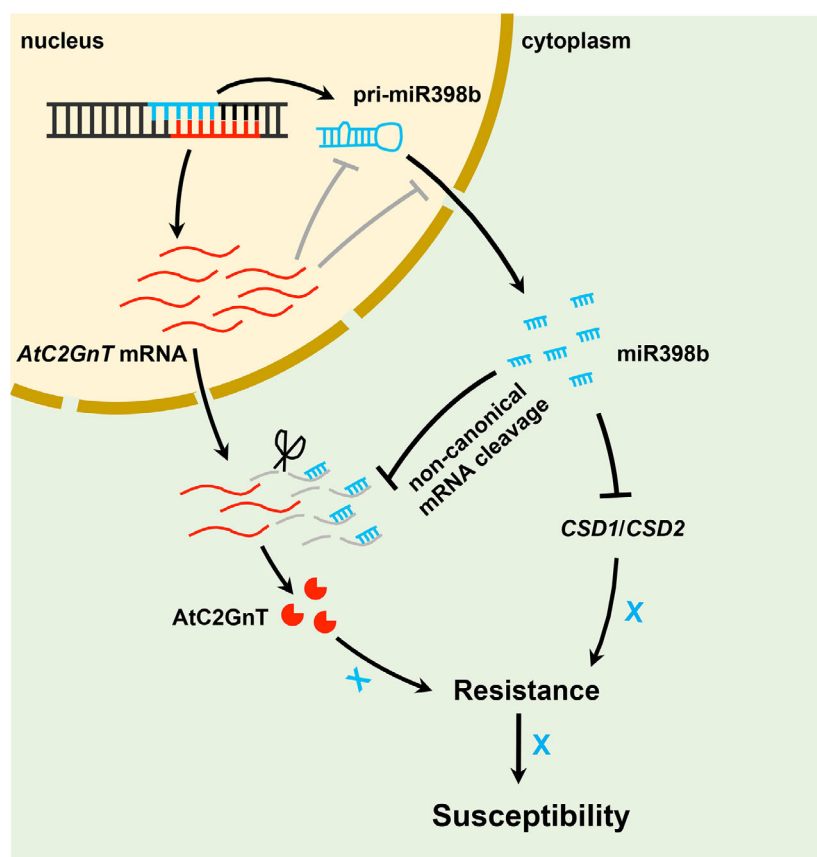
Despite the general belief that the majority of NATs in eukaryotes do not code for proteins (Jabnune et al., 2013), our study convincingly demonstrated that *AtC2GnT*, as the *cis*-NATs of *MIR398b*, could function at the protein level, which is supported by three lines of evidence. Firstly, a fusion protein, *C2GnT*-GFP, produced by transient expression in *N. benthamiana* was detected by Western blot, matching the anticipated molecular size of the fusion protein (Figure 4a). Secondly, *C2GnT*-GFP co-localized with the Golgi apparatus marker *CTS*-RFP (Figure 4b). Thirdly, the deletion mutant of *C2GnT*-GFP displayed altered subcellular localization and sensitivity to *P. parasitica*, indicating that the integrity of *AtC2GnT* is vital for its function (Figure 4c–f).

*AtC2GnT* was predicted to encode a Core-2/1-branching beta-1,6-*N*-acetylglucosaminyltransferase in the GT superfamily (Ye et al., 2011). GTs function to catalyze glycosylation, which is essential for the structural and functional diversity of glycoproteins (Eichler, 2019; Ohtsubo & Marth, 2006). GTs play multiple roles in the synthesis of complex cell wall polysaccharides, plant hormone homeostasis, stress tolerance, and plant defense (Vogt & Jones, 2000; Zhang et al., 2016; Zhao et al., 2020). For example, deficiency in the expression of *BC10*, which is a homologous gene of *AtC2GnT*, resulted in a weakened cell wall structure due to reductions in cellulose and arabinogalactan protein levels in *O. sativa* L. (Zhou et al., 2009). Similarly, *N*-acetylglucosaminyltransferase I (*GnTI*), which is essential for the processing of high-mannose to hybrid and complex *N*-glycans, was found to play an important role in salt tolerance (Kang et al., 2008; Strasser et al., 2006). In relevance to biotic stress, it was reported that the *N*-glycosylation of pattern recognition receptors was essential for microbe-associated molecular pattern-triggered plant immunity (Haweker et al., 2010). Such a concept was illustrated in a most recent study which reported that the pathogen-induced glycosyltransferase *UGT73C7* was able to promote Arabidopsis immunity via adjusting phenylpropanoid metabolism (Huang et al., 2021). In this study, our results corroborate the aforementioned studies and revealed that *AtC2GnT*, which encodes a Golgi-localized protein, could positively regulate plant resistance against *Phytophthora* pathogens. Future studies are warranted to further define the GT enzymatic activity and the donor and acceptor substrates of *AtC2GnT*, which shall shed more light on the molecular mechanisms underpinning *AtC2GnT*-directed plant immunity.

Based on our data, we propose a negative regulatory model between *AtC2GnT* and miR398b (Figure 6), in which miR398b mediates *A. thaliana* susceptibility to *P. parasitica* not only by suppressing the expression of *CSDs*, but also by suppressing *AtC2GnT* expression via guiding its mRNA cleavage; the *AtC2GnT* transcripts positively regulate *A. thaliana* resistance to *P. parasitica* via reported inhibition

**Figure 6.** Model of the *MIR398b* and *AtC2GnT* feedback loop in regulating plant immunity to *Phytophthora parasitica*.

miR398b mediates plant susceptibility to *P. parasitica* by suppressing the expression of *AtC2GnT*, *CSD1*, and *CSD2*. *AtC2GnT* transcripts enhance plant immunity via inhibition of the miR398b–CSDs module, by impairing the stability and accurate processing of pri-miR398b (Li et al., 2020), while *AtC2GnT* enhances plant immunity via its parallel route independent of the miR398b–CSDs pathway. *AtC2GnT*, encoding a core-2/1-branching beta-1,6-*N*-acetylglucosaminyltransferase, is a positive immune regulator in *Arabidopsis thaliana* to *P. parasitica*. *CSD1* and *CSD2*, encoding Cu/Zn-Superoxidase Dismutases, are also positive plant immune regulators. The gray line indicates suppression of miR398b–CSDs module activity by *AtC2GnT* transcripts, leading to impaired stability and accurate processing of pri-miR398b.



of the miR398b–CSDs module, by impairing the stability and accurate processing of pri-miR398b (Li et al., 2020), while *AtC2GnT* protein enhances plant resistance independently of the miR398b–CSDs pathway. Furthermore, both downregulation of miR398b and overexpression of *AtC2GnT* were able to enhance *P. parasitica* resistance without compromising plant growth (Figure S11), which is highly desired in crop breeding for disease resistance. In addition, as *MIR398b* and *AtC2GnT* are conserved in Brassicaceae (Yu et al., 2013), the illustration of the molecular relationship between *MIR398b* and *AtC2GnT* in *A. thaliana* may not only shed light on the plant immune responses to biotic and abiotic stress in various crops, but also pave the way for improving disease resistance in numerous economically important Brassicaceae crops, such as rapeseed (*Brassica napus*).

## EXPERIMENTAL PROCEDURES

### Plant materials and growth conditions

*Arabidopsis thaliana* Col-0 served as wild type in this study. The T-DNA insertion mutants *SALK\_109389C* for *CSD1* and *SALK\_041901C* for *CSD2* were purchased from AraShare (<https://www.arashare.cn/index/>). The *A. thaliana* seeds were surface-sterilized, planted, and vernalized as previously reported (Li, Zhao, et al., 2020; Wang et al., 2011). All the stable transgenic *A.*

*thaliana* lines were generated in the Col-0 background via the *A. tumefaciens*-mediated floral dip transformation method (Zhang et al., 2006). The generated transformants were screened on 1/2 Murashige and Skoog (MS) agar plates with kanamycin except for the CRISPR/Cas9-edited mutants, which were screened on 1/2 MS agar plates with hygromycin. PCR amplification and DNA sequencing analysis were employed to identify the CRISPR/Cas9-edited mutants. *Nicotiana benthamiana* was grown and maintained as previously reported (Huang et al., 2019).

### Plasmid construction

The pKannibal vector was digested at the *NotI* site, and the 3-kb fragment containing the CaMV 35S promoter, the *PDK* intron, and the *OCS* terminator was inserted into the pART27 vector (Gleave, 1992), and the new vector was named PAKK. To generate the G:U hpRNA vector, the G:U hpRNA fragment (Zhong, 2019), which harbors two miR398b target sites, was synthesized by Wuhan GeneCreate Biological Engineering Co., Ltd. (Wuhan, Hubei, China). The fragment was inserted between the *EcoRI*/*HindIII* sites of PAKK. For construction of *p35S::AtC2GnT*, the CDS of *AtC2GnT* was cloned from wild-type (Col-0) cDNA by gene-specific primers, and the fragment was inserted between the *EcoRI*/*HindIII* sites of PAKK. To generate *p35S::miR398b*, we amplified the genomic sequence containing pre-miR398b from Col-0 genomic DNA (gDNA) with gene-specific primers. The amplified fragment was cloned between the *EcoRI*/*XbaI* sites of PAKK. To generate the amiR398b construct, the miR319a backbone (Schwab et al., 2006) was used to clone the miR398b precursor into the PAKK vector. The fusion fragments C2GnT-GFP and CTS-RFP, generated by overlapping PCR, were inserted between the *EcoRI*/*XhoI*

sites of PAK. For construction of the deletion mutants, the sequences were cloned from the *p35S::AtC2GnT* plasmid by gene-specific primers. To generate the RNAi construct, the fragments were inserted between the *XhoI/EcoRI* sites and the *XbaI/HindIII* sites of binary vector PAK, respectively. For construction of *pTRV2::NbC2GnT*, a 173-bp cDNA fragment of *NbC2GnT* was cloned from the *N. benthamiana* cDNA. The fragment was inserted into the TRV2 vector between the *XbaI/BamHI* sites. In order to generate GFP-tagged 3'-UTRs of *AtC2GnT*, the GFP fragment was inserted between the *XhoI/HindIII* sites of binary vector PAK, and the new vector was named PAK-GFP. We obtained the wild-type 3'-UTR of *AtC2GnT* at its C-terminus (*p35S::GFP-wtUTR*) or a mutated 3'-UTR containing an altered miR398b target site (*p35S::GFP-wtUTR*) using gene-specific primers. The amplified fragments were inserted between the *HindIII/XbaI* sites of binary vector PAK-GFP.

To generate the CRISPR/Cas9 construct, two sgRNAs (sgRNA1 and sgRNA2) targeting the CDS of *AtC2GnT* were screened by CRISPRdirect (<http://crispr.dbcls.jp/>) (Naito et al., 2014). The sgRNAs were inserted into the psgR-Cas9-At backbone as previously reported (Mao et al., 2013). The fragment carrying the sgRNAs and *Cas9* were inserted between the *HindIII/EcoRI* sites of binary vector PCXSN as previously described (Lu et al., 2020). All primers used in this study are listed in Table S1.

#### qRT-PCR analysis

All cDNAs were generated by the Evo M-MLV RT Kit with gDNA Clean for qPCR (Accurate Biology, Changsha, Hunan, China). The qRT-PCR reactions were conducted using UltraSYBR Mixture (CWVIO, Beijing, China). Primers used for qRT-PCR analysis are listed in Table S1.

#### RLM-5' RACE analysis

RLM-5' RACE was performed with the FirstChoice® RLM-RACE Kit (Invitrogen™, Carlsbad, CA, USA) according to a modified user manual to identify the cleavage site of miR398b in *AtC2GnT*. Total RNA was extracted from miR398b overexpression transgenic plants. The gDNA was cleaned with the Evo M-MLV RT Kit with gDNA Clean for qPCR (Accurate Biology, Changsha, Hunan, China). The 5' RACE adapter was ligated to the degraded mRNAs with T4 RNA ligase. Reverse transcription was performed with Oligo dT (18T). The primers for nested PCR are listed in Table S1; the sequencing results are listed in Figure S2.

#### Transient expression assays

The *A. tumefaciens*-mediated transient expression assays in *N. benthamiana* were conducted as previously reported (Huang et al., 2019; Li, Wang, et al., 2019). Briefly, *A. tumefaciens* strain GV3101 cells harboring the respective constructs were cultured in Luria-Bertani medium with appropriate antibiotics at 28°C for 24 h, followed by centrifugation for 5 min at 4000 *g* at room temperature. The harvested bacterial cells were resuspended and diluted to the appropriate OD<sub>600</sub> with infiltration buffer (10 mM MES, 10 mM MgCl<sub>2</sub>, and 0.2 mM acetosyringone, pH 5.6). The resuspended bacteria were infiltrated into the abaxial side of 5–6-week-old *N. benthamiana* leaves.

#### Fluorescence microscopy

Confocal images of *N. benthamiana* epidermal cells were taken at about 3 days after agroinfiltration using an Olympus FV3000 confocal microscope (Olympus, Tokyo, Japan) and a ZEISS LSM 900 microscope with Airyscan 2 (Zeiss, Oberkochen, Germany).

ER-mCherry (Fan et al., 2018) was used as ER marker; CTS-RFP was used as Golgi marker (Strasser et al., 2006).

#### VIGS assay in *N. benthamiana*

The VIGS assays in *N. benthamiana* were conducted as previously reported (Liu et al., 2002; Ratcliff et al., 2001). Briefly, *A. tumefaciens* carrying vector pTRV1 was mixed with strains harboring *pTRV2::GFP*, *pTRV2::NbC2GnT*, and *pTRV2::PDS* constructs in equal ratios to a final concentration of OD<sub>600</sub> = 0.2. As previously described, four-leaf-stage *N. benthamiana* seedlings were used for VIGS (Huang et al., 2019; Ratcliff et al., 2001). The silenced plants were challenged with *P. parasitica* or *P. infestans* 3 weeks post-infiltration.

#### Pathogen cultural conditions and inoculation

Strain Pp016-GFP was used for *P. parasitica* inoculation assays. Strain culture and production of zoospores were conducted as described in a previous study (Wang et al., 2011). Strain Pi88069 was used for the *P. infestans* inoculation assay. Strain culture and production of zoospores were performed as previously reported (Li, Zhao, et al., 2020; Wang et al., 2015).

The inoculation assay for *P. parasitica* in *A. thaliana* was conducted as follows. Four-week-old detached leaves of *A. thaliana* were inoculated with a 13- $\mu$ l droplet containing  $2 \times 10^3$  *P. parasitica* zoospores. The plant disease symptoms were observed at 3 dpi. The statistical analysis of plant disease grades was based on the Wilcoxon rank-sum test (Huang et al., 2019; Li, Zhao, et al., 2020). The inoculation assay for *P. parasitica* in *N. benthamiana* was conducted using detached leaves of *N. benthamiana* that were inoculated with fresh mycelia of Pp016-GFP that were grown on 5% CA medium (Wang et al., 2011). The lesion diameters in the infected leaves were measured at 60 hpi. The inoculation assay for *P. infestans* in *N. benthamiana* leaves was conducted using detached leaves of respective plants, which were challenged with a 16- $\mu$ l droplet containing  $1 \times 10^3$  *P. infestans* zoospores. The diameters of lesions were measured at 6–7 dpi. More than 10 leaves were used for statistical analysis based on Student's *t*-test. The pathogenicity assays were repeated at least three times.

#### Statistical analysis

The statistical analysis for gene expression, biomass, and lesion diameters was based on Student's *t*-test. The statistical analysis of plant disease grades was based on the Wilcoxon rank-sum test. Asterisks indicate significant differences (\**P* < 0.05, \*\**P* < 0.01, \*\*\**P* < 0.001).

#### ACCESSION NUMBERS

Accession numbers are as follows: *AtC2GnT*, At5G14550; *MIR398b*, At5G14545; *CSD1*, At1G08830; *CSD2*, At2G28190; *NbC2GnTA*, Niben101Scf11415g00001.1; *NbC2GnTB*, Niben101Scf01448g02029.1.

#### ACKNOWLEDGMENTS

We would like to thank Dr. Ming-Bo Wang (CSIRO Agriculture, Canberra, Australia) and Dr. Jin-Bu Jia (Institute of Plant and Food Science, Southern University of Science and Technology, Shenzhen, China) for their helpful suggestions on the manuscript. This work was supported by the China Agriculture Research System (CARS-09), the National Natural Science Foundation of China (31930094), and the Programme of Introducing Talents of Innovative Discipline to Universities (project 111) from the State Administration of Foreign Experts Affairs (#B18042).

## AUTHOR CONTRIBUTIONS

WS and XG designed the research. CZ, PZ, LM, YL, WL, JZ, JX, and YM performed the experiments. XG, CZ, and WS analyzed the data. XG and WS wrote the manuscript with contributions from all authors.

## CONFLICT OF INTEREST

All the authors declare that they have no competing interests.

## DATA AVAILABILITY STATEMENT

The data that support the findings of this study are available from the corresponding author upon reasonable request.

## SUPPORTING INFORMATION

Additional Supporting Information may be found in the online version of this article.

**Table S1.** Primers used in this study.

**Figure S1.** *Arabidopsis thaliana* CSD1 and CSD2 are positive regulators of plant resistance to *Phytophthora parasitica*.

**Figure S2.** Sequencing analysis of the miR398b-guided *AtC2GnT* transcript cleavage site.

**Figure S3.** Silencing of *AtC2GnT* enhanced plant susceptibility to *Phytophthora parasitica*.

**Figure S4.** Relative expression levels of related genes in RNAi transgenic lines, the *c2gnt* mutant, and *AtC2GnT*-overexpressing transgenic plants.

**Figure S5.** Transient expression of *AtC2GnT* in *Nicotiana benthamiana* enhanced plant resistance to *Phytophthora* pathogens.

**Figure S6.** Fluorescence distribution of C2GnT-GFP in *Nicotiana benthamiana* epidermal cells.

**Figure S7.** Phylogenetic analysis of the GT14/GT14-like family in *Arabidopsis thaliana*.

**Figure S8.** Analysis of *AtC2GnT* protein.

**Figure S9.** NT-GFP was partially localized in the ER.

**Figure S10.** Homologs of *AtC2GnT* in *Nicotiana benthamiana*.

**Figure S11.** The growth phenotypes of miR398b-silenced and *AtC2GnT* overexpression *Arabidopsis thaliana* transgenic plants.

## REFERENCES

- Brodersen, P., Sakvarelidze-Achard, L., Bruun-Rasmussen, M., Dunoyer, P., Yamamoto, Y.Y., Sieburth, L. *et al.* (2008) Widespread translational inhibition by plant miRNAs and siRNAs. *Science*, **320**, 1185–1190.
- Eichler, J. (2019) Protein glycosylation. *Current Biology*, **29**, 229–231.
- Fan, G., Yang, Y., Li, T., Lu, W., Du, Y., Qiang, X. *et al.* (2018) A *Phytophthora capsici* RXLR effector targets and inhibits a plant PPlase to suppress endoplasmic reticulum-mediated immunity. *Molecular Plant*, **11**, 1067–1083.
- Gleave, A.P. (1992) A versatile binary vector system with a T-DNA organisational structure conducive to efficient integration of cloned DNA into the plant genome. *Plant Molecular Biology*, **20**, 1203–1207.
- Guan, Q., Lu, X., Zeng, H., Zhang, Y. & Zhu, J. (2013) Heat stress induction of *miR398* triggers a regulatory loop that is critical for thermotolerance in *Arabidopsis*. *The Plant Journal*, **74**, 840–851.
- Hawker, H., Rips, S., Koiwa, H., Salomon, S., Saijo, Y., Chinchilla, D. *et al.* (2010) Pattern recognition receptors require *N*-glycosylation to mediate plant immunity. *Journal of Biological Chemistry*, **285**, 4629–4636.
- Huang, G., Liu, Z., Gu, B., Zhao, H., Jia, J., Fan, G. *et al.* (2019) An RXLR effector secreted by *Phytophthora parasitica* is a virulence factor and

triggers cell death in various plants. *Molecular Plant Pathology*, **20**, 356–371.

- Huang, X.X., Wang, Y., Lin, J.S., Chen, L., Li, Y.J., Liu, Q. *et al.* (2021) The novel pathogen-responsive glycosyltransferase UGT73C7 mediates the redirection of phenylpropanoid metabolism and promotes *SNC1*-dependent *Arabidopsis* immunity. *The Plant Journal*, **107**, 149–165.
- Jabnounge, M., Secco, D., Lecampion, C., Robaglia, C., Shu, Q. & Poirier, Y. (2013) A rice *cis*-natural antisense RNA acts as a translational enhancer for its cognate mRNA and contributes to phosphate homeostasis and plant fitness. *The Plant Cell*, **25**, 4166–4182.
- Jagadeeswaran, G., Saini, A. & Sunkar, R. (2009) Biotic and abiotic stress down-regulate miR398 expression in *Arabidopsis*. *Planta*, **229**, 1009–1014.
- Jiang, M., Chen, H., Liu, J., Du, Q., Lu, S. & Liu, C. (2021) Genome-wide identification and functional characterization of natural antisense transcripts in *Salvia miltiorrhiza*. *Scientific Reports*, **11**, 4769.
- Jiang, N., Cui, J., Hou, X., Yang, G., Xiao, Y., Han, L. *et al.* (2020) Sl-lncRNA15492 interacts with Sl-miR482a and affects *Solanum lycopersicum* immunity against *Phytophthora infestans*. *The Plant Journal*, **103**, 1561–1574.
- Jin, H., Vacic, V., Girke, T., Lonardi, S. & Zhu, J.K. (2008) Small RNAs and the regulation of *cis*-natural antisense transcripts in *Arabidopsis*. *BMC Molecular Biology*, **9**, 6.
- Jones-Rhoades, M.W., Bartel, D.P. & Bartel, B. (2006) MicroRNAs and their regulatory roles in plants. *Annual Review of Plant Biology*, **57**, 19–53.
- Judelson, H.S. & Blanco, F.A. (2005) The spores of *Phytophthora*: weapons of the plant destroyer. *Nature Reviews Microbiology*, **3**, 47–58.
- Kamoun, S., Furzer, O., Jones, J.D., Judelson, H.S., Ali, G.S., Dalio, R.J. *et al.* (2015) The top 10 oomycete pathogens in molecular plant pathology. *Molecular Plant Pathology*, **16**, 413–434.
- Kang, J.S., Frank, J., Kang, C.H., Kajjura, H., Vikram, M., Ueda, A. *et al.* (2008) Salt tolerance of *Arabidopsis thaliana* requires maturation of *N*-glycosylated proteins in the Golgi apparatus. *Proceedings of the National Academy of Sciences of the United States of America*, **105**, 5933–5938.
- Katiyar-Agarwal, S. & Jin, H. (2010) Role of small RNAs in host-microbe interactions. *Annual Review of Phytopathology*, **48**, 225–246.
- Lee, H.J., Park, Y.J., Kwak, K.J., Kim, D., Park, J.H., Lim, J.Y. *et al.* (2015) MicroRNA844-guided downregulation of cytidinephosphate diacylglycerol synthase3 (CDS3) mRNA affects the response of *Arabidopsis thaliana* to bacteria and fungi. *Molecular Plant-Microbe Interactions*, **28**, 892–900.
- Li, T., Wang, Q., Feng, R., Li, L., Ding, L., Fan, G. *et al.* (2019) Negative regulators of plant immunity derived from cinnamyl alcohol dehydrogenases are targeted by multiple *Phytophthora* Avr3a-like effectors. *New Phytologist*. Available from: <https://doi.org/10.1111/nph.16139>.
- Li, W., Zhao, D., Dong, J., Kong, X., Zhang, Q., Li, T. *et al.* (2020) *AtRTP5* negatively regulates plant resistance to *Phytophthora* pathogens by modulating the biosynthesis of endogenous jasmonic acid and salicylic acid. *Molecular Plant Pathology*, **21**, 95–108.
- Li, Y., Cao, X.L., Zhu, Y., Yang, X.M., Zhang, K.N., Xiao, Z.Y. *et al.* (2019) *Osa-miR398b* boosts H<sub>2</sub>O<sub>2</sub> production and rice blast disease-resistance via multiple superoxide dismutases. *New Phytologist*, **222**, 1507–1522.
- Li, Y., Lu, Y., Shi, Y., Wu, L., Xu, Y., Huang, F. *et al.* (2014) Multiple rice microRNAs are involved in immunity against the blast fungus *Magnaporthe oryzae*. *Plant Physiology*, **164**, 1077–1092.
- Li, Y., Zhang, Q., Zhang, J., Wu, L., Qi, Y. & Zhou, J.M. (2010) Identification of microRNAs involved in pathogen-associated molecular pattern-triggered plant innate immunity. *Plant Physiology*, **152**, 2222–2231.
- Li, Y.J., Li, X.R., Yang, J. & He, Y.K. (2020) Natural antisense transcripts of *MIR398* genes suppress microR398 processing and attenuate plant thermotolerance. *Nature Communications*, **11**, 5351.
- Lin, K.Y., Wu, S.Y., Hsu, Y.H. & Lin, N.S. (2022) MiR398-regulated antioxidants contribute to bamboo mosaic virus accumulation and symptom manifestation. *Plant Physiology*, **188**, 593–607.
- Liu, J., Fan, H., Wang, Y., Han, C., Wang, X., Yu, J. *et al.* (2020) Genome-wide microRNA profiling using oligonucleotide microarray reveals regulatory networks of microRNAs in *Nicotiana benthamiana* during beet necrotic yellow vein virus infection. *Viruses*, **12**, 310.
- Liu, Y., Schiff, M., Marathe, R. & Dinesh-Kumar, S.P. (2002) Tobacco *Rar1*, *EDS1* and *NPR1/NIM1* like genes are required for *N*-mediated resistance to tobacco mosaic virus. *The Plant Journal*, **30**, 415–429.

- Lu, W., Deng, F., Jia, J., Chen, X., Li, J., Wen, Q. *et al.* (2020) The *Arabidopsis thaliana* gene *AtERF019* negatively regulates plant resistance to *Phytophthora parasitica* by suppressing PAMP-triggered immunity. *Molecular Plant Pathology*, **21**, 1179–1193.
- Mao, Y., Xu, J., Wang, Q., Li, G., Tang, X., Liu, T. *et al.* (2021) A natural antisense transcript acts as a negative regulator for the maize drought stress response gene *ZmNAC48*. *Journal of Experimental Botany*, **72**, 2790–2806.
- Mao, Y., Zhang, B., Gou, F., Zhang, H., Xua, N. & Zhu, J.K. (2013) Application of the CRISPR-Cas system for efficient genome engineering in plants. *Molecular Plant*, **6**, 2008–2011.
- Naito, Y., Hino, K., Bono, H. & Ui-Tei, K. (2014) CRISPRdirect: software for designing CRISPR/Cas guide RNA with reduced off-target sites. *Bioinformatics*, **31**, 1120–1123.
- Niu, D., Lii, Y.E., Chellappan, P., Lei, L., Peralta, K., Jiang, C. *et al.* (2016) miRNA863-3p sequentially targets negative immune regulator *ARLPKs* and positive regulator *SERRATE* upon bacterial infection. *Nature Communications*, **7**, 11324.
- Ohtsubo, K. & Marth, J.D. (2006) Glycosylation in cellular mechanisms of health and disease. *Cell*, **126**, 855–867.
- Ratcliff, F., Martin-Hernandez, A.M. & Baulcombe, D.C. (2001) Tobacco rattle virus as a vector for analysis of gene function by silencing. *The Plant Journal*, **25**, 237–245.
- Ren, Y., Li, M., Wang, W., Lan, W., Schenke, D., Cai, D. *et al.* (2022) MicroRNA840 (*MIR840*) accelerates leaf senescence by targeting the overlapping 3' UTRs of *PPR* and *WHIRLY3* in *Arabidopsis thaliana*. *The Plant Journal*, **109**, 126–143.
- Roskiewicz, W. & Makalowska, I. (2016) Biological functions of natural antisense transcripts. *Acta Biochimica Polonica*, **63**, 665–673.
- Schwab, R., Ossowski, S., Rießer, M., Warthmann, N. & Weigel, D. (2006) Highly specific gene silencing by artificial microRNAs in *Arabidopsis*. *The Plant Cell*, **18**, 1121–1133.
- Šečić, E., Kogel, K.H. & Ladera-Carmona, M.J. (2021) Biotic stress-associated microRNA families in plants. *Journal of Plant Physiology*, **263**, 153451.
- Song, L., Fang, Y., Chen, L., Wang, J. & Chen, X. (2021) Role of non-coding RNAs in plant immunity. *Plant Communications*, **2**, 100180.
- Strasser, R., Schoberer, J., Jin, C., Glossl, J., Mach, L. & Steinkellner, H. (2006) Molecular cloning and characterization of *Arabidopsis thaliana* Golgi  $\alpha$ -mannosidase II, a key enzyme in the formation of complex N-glycans in plants. *The Plant Journal*, **45**, 789–803.
- Su, W.Y., Li, J.T., Cui, Y., Hong, J., Du, W., Wang, Y.C. *et al.* (2012) Bidirectional regulation between *WDR83* and its natural antisense transcript *DHPS* in gastric cancer. *Cell Research*, **22**, 1374–1389.
- Sunkar, R., Kapoor, A. & Zhu, J. (2006) Posttranscriptional induction of two Cu/Zn superoxide dismutase genes in *Arabidopsis* is mediated by down-regulation of miR398 and important for oxidative stress tolerance. *The Plant Cell*, **18**, 2051–2065.
- Teasdale, R.D., Matheson, F. & Gleeson, P.A. (1994) Post-translational modifications distinguish cell surface from Golgi-retained  $\beta$ 1,4 galactosyltransferase molecules. Golgi localization involves active retention. *Glycobiology*, **4**, 917–928.
- Thines, M. & Kamoun, S. (2010) Oomycete-plant coevolution: recent advances and future prospects. *Current Opinion in Plant Biology*, **13**, 427–433.
- Vogt, T. & Jones, P. (2000) Glycosyltransferases in plant natural product synthesis: characterization of a supergene family. *Trends in Plant Science*, **5**, 380–386.
- Wang, X., Boevink, P., McLellan, H., Armstrong, M., Bukharova, T., Qin, Z. *et al.* (2015) A host KH RNA-binding protein is a susceptibility factor targeted by an RXLR effector to promote late blight disease. *Molecular Plant*, **8**, 1385–1395.
- Wang, X.J., Gaasterland, T. & Chua, N.H. (2005) Genome-wide prediction and identification of cis-natural antisense transcripts in *Arabidopsis thaliana*. *Genome Biology*, **6**, R30.
- Wang, Y., Meng, Y., Zhang, M., Tong, X., Wang, Q., Sun, Y. *et al.* (2011) Infection of *Arabidopsis thaliana* by *Phytophthora parasitica* and identification of variation in host specificity. *Molecular Plant Pathology*, **12**, 187–201.
- Wight, M. & Werner, A. (2013) The functions of natural antisense transcripts. *Essays in Biochemistry*, **54**, 91–101.
- Xu, W.H., Meng, Y. & Wise, R.P. (2014) *Mla*- and *Rom1*-mediated control of microRNA398 and chloroplast copper/zinc superoxide dismutase regulates cell death in response to the barley powdery mildew fungus. *New Phytologist*, **201**, 1396–1412.
- Ye, C.Y., Li, T., Tuskan, G.A., Tschaplinski, T.J. & Yang, X. (2011) Comparative analysis of GT14/GT14-like gene family in *Arabidopsis*, *Oryza*, *Populus*, *Sorghum* and *Vitis*. *Plant Science*, **181**, 688–695.
- Yu, X., Yang, J., Li, X.R., Liu, X.X., Sun, C.B., Wu, F.J. *et al.* (2013) Global analysis of cis-natural antisense transcripts and their heat-responsive nat-siRNAs in *Brassica rapa*. *BMC Plant Biology*, **13**, 208.
- Yu, Y., Jia, T. & Chen, X. (2017) The 'how' and 'where' of plant microRNAs. *New Phytologist*, **216**, 1002–1017.
- Zhang, M., Wei, F., Guo, K., Hu, Z., Li, Y., Xie, G. *et al.* (2016) A novel *FC116/BC10* mutation distinctively causes alteration in the expression of the genes for cell wall polymer synthesis in Rice. *Frontiers in Plant Science*, **7**, 1366.
- Zhang, X., Henriques, R., Lin, S.S., Niu, K.W. & Chua, N.H. (2006) *Agrobacterium*-mediated transformation of *Arabidopsis thaliana* using the floral dip method. *Nature Protocols*, **1**, 641–646.
- Zhao, J.N., Wang, R.F., Zhao, S.J. & Wang, Z.T. (2020) Advance in glycosyltransferases, the important bioparts for production of diversified ginsenosides. *Chinese Journal of Natural Medicines*, **18**, 643–658.
- Zhong, C. (2019) *Identification and functional characterization of Arabidopsis small RNAs in response to Phytophthora infection*. PhD thesis. Yangling: The Northwest A&F University.
- Zhou, Y., Li, S., Qian, Q., Zeng, D., Zhang, M., Guo, L. *et al.* (2009) BC10, a DUF266-containing and Golgi-located type II membrane protein, is required for cell-wall biosynthesis in rice (*Oryza sativa* L.). *The Plant Journal*, **57**, 446–462.
- Zhu, X., He, S., Fang, D., Guo, L., Zhou, X., Guo, Y. *et al.* (2020) High-throughput sequencing-based identification of *Arabidopsis* miRNAs induced by *Phytophthora capsici* infection. *Frontiers in Microbiology*, **11**, 1094.